Sense and non-sense of shear in flanking structures

Bernhard Grasemann[a,*], Kurt Stüwe[b], Jean-Claude Vannay[c]

[a]*Institut für Geologie, University of Vienna, A-1090 Vienna, Austria*
[b]*Institut für Geologie und Paläontologie, University of Graz, A-8010 Graz, Austria*
[c]*Institut de Minéralogie et Pétrographie, Université de Lausanne, CH-1015 Lausanne, Switzerland*

Abstract

The deformation of marker horizons across slip surfaces can lead to the development of several types of *flanking structures*. The development of such structures was investigated using a numerical model to simulate the flow around a slip surface in a viscous medium. The modelled structures can be classified on the basis of three criteria: (1) the extensional or contractional offset of markers, (2) the co- or counter-shearing sense along the slip surfaces and (3) the normal or reverse drag of markers relative to the shear sense along the slip surfaces. As a function of the kinematic vorticity of the flow and the initial orientation of the slip surface, with respect to the shear zone boundaries, three main types of structures can develop: (1) *shear bands* developed along co-shearing extensional slip surfaces; (2) *a-type flanking folds* developed along counter-shearing slip surfaces; and (3) *s-type flanking folds* developed along co-shearing contractional slip surfaces. All these structures can occur with either normal or reverse drag effects. Shear bands and a-type flanking folds recording opposite shear senses can be geometrically very similar and consequently lead to kinematic misinterpretations. However, correctly identified flanking structures can provide quantitative information about the kinematic vorticity of the flow. © 2002 Elsevier Science Ltd. All rights reserved.

Keywords: Shear sense indicator; Finite element modelling; Shear band; Flanking structures; General shear deformation

1. Introduction

Ductile shear zones often contain discrete internal slip surfaces oblique with respect to the shear zone boundaries and generally dipping in the direction of the shear. These slip surfaces are referred to as C'-surfaces (Berthé et al., 1979), shear bands (White, 1979) or extensional crenulation cleavage (Platt and Vissers, 1980), and they are frequently used as kinematic indicators. Because these slip surfaces often make a small angle (~ 25–$30°$) with respect to the shear zone boundaries, they are thought to represent an irrotational direction of the flow. Consequently they have been interpreted as being parallel to the shortening eigenvector of a general shear flow (Simpson and De Paor, 1993; Pray et al., 1997). The kinematic interpretation of shear zones can, however, be hindered by the presence of slip surfaces recording an opposite sense of shear with respect to the regional shear sense (Platt and Vissers, 1980; Behrmann, 1987; Ramsay and Lisle, 2000). Furthermore, these slip systems

may co- or counter-rotate during progressive deformation (Platt, 1984; Stock, 1992) and are thought to be indicative of general shear flow (Platt and Vissers, 1980).

An additional problem is that the deflection of marker horizons adjacent to some slip surfaces indicates an opposite shear sense relative to the displacement revealed by the offset of such marker horizons. Such structures, characterised by an inconsistent drag of marker horizons, are observed in various natural settings (Grasemann and Stüwe, 2001; Passchier, 2001), as well as in analogue (Baumann, 1986; Hudleston, 1989; Odonne, 1990) and numerical models of faults in elastic materials (Baumann, 1986; Reches and Eidelman, 1995). Such features indicate that 'classical' shear bands (i.e. C'-surfaces) represent only one example of several types of structures along slip surfaces that can develop during progressive deformation. Therefore, the general name of *flanking structures* (Passchier, 2001) has been recently introduced for the deflection of the fabric of rocks (e.g. foliation or layering) near the margin of cross-cutting elements (CE). CE corresponds to a cross-cutting planar feature (e.g. fault, vein or dyke) embedded in a layered rock referred to as the host element (HE; see Fig. 1).

Using numerical modelling Grasemann and Stüwe

* Corresponding author. Tel.: +43-1-4277-53472; fax: +43-1-4277-9534.

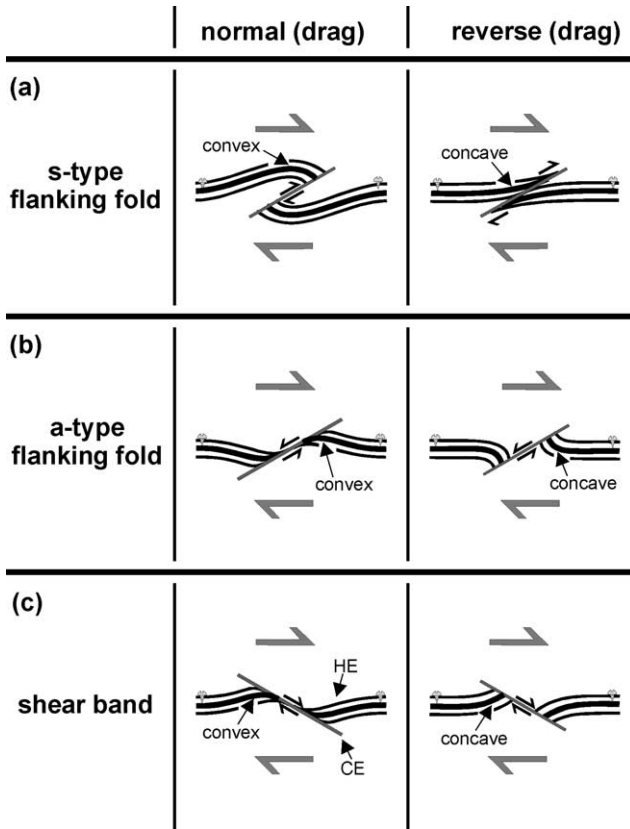*E-mail address:* bernhard.grasemann@univie.ac.at (B. Grasemann).

Fig. 1. Terminology of the flanking structures discussed in the present study. HE—host element containing marker horizons parallel to the shear zone boundaries; CE—cross-cutting element, i.e. a planar slip surface embedded in the HE. The convex or concave deflection of the marker line in the direction of shear along CE defines normal or reverse drag. (a) s-Type flanking folds are co-shearing with a contractional offset, (b) a-type flanking folds are counter-shearing; and (c) shear bands are co-shearing with an extensional offset.

(2001) investigated the deflection and offset of marker horizons around a CE simulating a tension gash initially oriented at 45° with respect to the boundaries of the shear zone deforming by simple shear. This modelling showed that, during progressive deformation, the drag of the marker horizons associated with the rotation and shear of the CE leads to the formation of an antiform–synform fold train. For a rheologically strong CE, no offset of the marker horizons occurs at the CE. In contrast, a rheologically weak CE leads to the development of a slip surface recording a displacement in the opposite sense relative to the bulk shear flow. Consequently, although the drag of the marker horizons is consistent with the main shear sense, it is inconsistent with the shear sense along the CE. These results show that a correct kinematic interpretation requires a careful analysis of the deflection of marker horizons.

The present study addresses the deformation around slip surfaces (CE) embedded in a ductile rock (HE) as a function of the type of ductile flow and of the initial orientation of CE. The full range of isochoric plane strain

flow conditions between the end members simple and pure shear is investigated. Deformation is applied for the complete range of initial CE orientations, whereas marker horizons in the HE are initially parallel to the shear zone boundaries. These conditions generate a spectrum of flanking structures that can be subdivided into *shear bands*, *a-* and *s-type flanking folds*, all of them showing either a normal or a reverse drag (Fig. 1). The aim of this study is to describe the instantaneous and finite kinematic development of these flanking structures on the basis of a comparison between the results of finite element modelling and natural examples.

2. Numerical technique

In order to investigate the range of flanking structures developing within a linear viscous medium (HE) around an active but pinned slip surface (CE), we use the two-dimensional finite element model BASIL of Barr and Houseman (1992, 1996). The modelling methodology is comparable with that presented in Grasemann and Stüwe (2001) but differs in three aspects: (1) we model only linear viscous material because non-linear and linear rheologies generate topologically equivalent structures (Grasemann and Stüwe, 2001); (2) we investigate only the deformation around an infinitely thin free-slipping surface embedded in a viscous medium; and (3) the conditions are relaxed to include general shear.

2.1. Rheology

For a linear viscous rheology stress is proportional to strain rate:

$$\tau_{ij} = 2\eta\dot{\epsilon}_{ij} \tag{1}$$

where τ_{ij} are the deviatoric components of the stress tensor, $\dot{\epsilon}_{ij}$ are the components of the strain rate tensor and η is the viscosity. The strain rate is defined in terms of the components of velocity u, in the spatial x_i- and x_j-directions:

$$\dot{\epsilon}_{ij} = \frac{1}{2}\left[\frac{\partial u_i}{\partial x_j} + \frac{\partial u_j}{\partial x_i}\right] \tag{2}$$

BASIL calculates incompressible plane strain deformation by using Eq. (1) with the force balance equations in two dimensions:

$$\frac{\partial}{\partial x_j}\tau_{ij} + \frac{\partial}{\partial x_i}p = 0 \tag{3}$$

where the summation is over the i and j indices and p is the pressure.

2.2. Geometry of the CE

The numerical model was set up to describe flow disturbances around pre-existing slip surfaces. The development of CE is not considered here and discussed elsewhere (e.g.
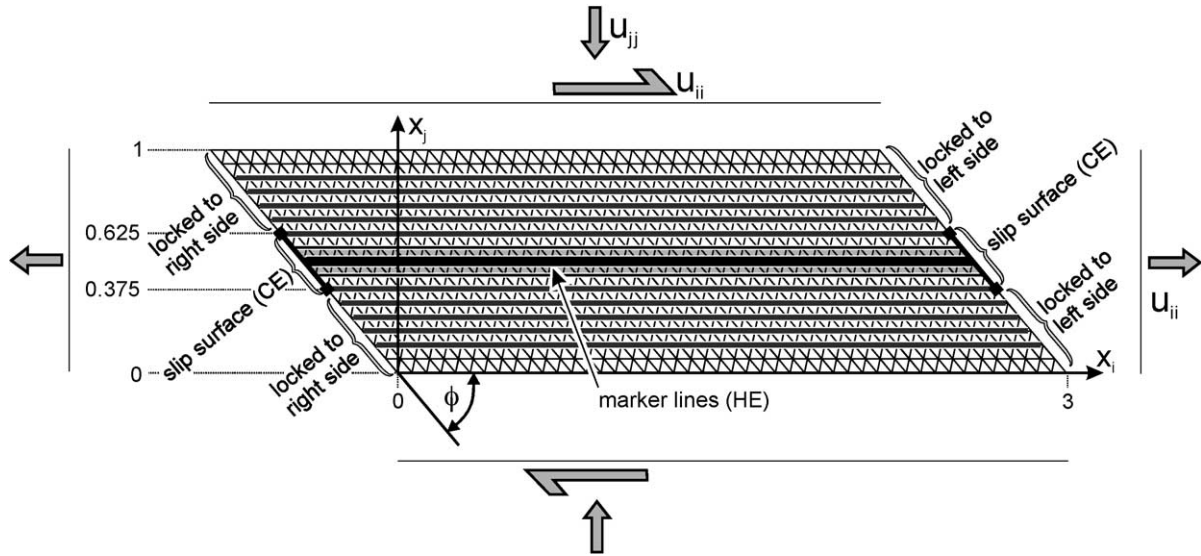
Fig. 2. Initial set-up and boundary conditions for the finite element model. The grid includes 48 by 16 elements. Stress and strain are continuous across the lateral boundaries except in the central 25% where deformation is discontinuous (see text). Velocities applied at the upper and lower boundaries of the grid allow a wide range of flow types. The variable fault-tilt angle ϕ defines the initial orientation of the CE.

Platt, 1984; Harris and Cobbold, 1985; Dennis and Secor, 1987; Jiang and White, 1995). The deformation is partitioned between the slip surface and continuous deformation in the matrix. The latter can be separated into a background strain induced by the boundary conditions and a perturbation strain (e.g. Mancktelow, 1991). The model includes a region with 48 by 16 elements in the two spatial directions (Fig. 2). The left side of the modelled region was numerically welded to the right side, so that all components of stress and deformation are continuous across this boundary in order to simulate an infinite periodic shear zone. This condition was relaxed in the central 25% of the lateral boundary of the grid, where we assume that: (i) the shear stress on the fault is zero; (ii) the normal stress across the fault is continuous; and (iii) the velocity normal to the fault is continuous but otherwise unconstrained. This corresponds to a pinned slip surface along the side of the modelled region. Overall, this starting geometry simulates an infinitely long shear zone, with internal slip surfaces repeated at distances corresponding to three shear zone widths and oriented at angle ϕ to the shear zone boundaries. The robustness of these assumptions for shorter slip surfaces, finer grid spacing and other aspect ratios was tested to ensure that the simulations represent a close approximation of the deformation of a finite length fault unaffected by the thickness of the shear zone.

The assumption of zero shear stress along the slip surface is not necessarily a realistic approximation of natural behaviour in rocks, but it is convenient for the purpose of assessing the influence of the slip along a CE on the deformation of the surrounding HE. Increasing the friction along the slip surface would result in a smaller slip, and therefore in a less pronounced drag of marker lines in the HE (Reches and

Eidelman, 1995). Marker horizons in the HE simulate a foliation or layering that is initially parallel to the shear zone boundaries, and consequently to the fabric attractor of the flow (Passchier, 1987).

2.3. Boundary conditions

The displacement boundary conditions at the top and bottom of the modelled shear zone are velocities. The components of the velocity gradient tensor L for homogeneous isochoric plane strain flow, where the stretching eigenvector of the flow is parallel to the shear zone boundaries, are:

$$L_{ij} = \begin{pmatrix} \dfrac{\partial u_i}{\partial x_i} & \dfrac{\partial u_i}{\partial x_j} \\ 0 & \dfrac{\partial u_j}{\partial x_j} \end{pmatrix} \tag{4}$$

where:

$$\frac{\partial u_i}{\partial x_i} = -\frac{\partial u_j}{\partial x_j}$$

Because we want to compare finite structures developing during different flow types, between the pure and simple shear end-members, it is critical to find components of L resulting in comparable finite deformation. However, there is no general agreement about what boundary conditions lead to equivalent finite deformation for different flow geometries (e.g. Fossen and Tikoff, 1997; Jiang, 1998). For the present study we used velocities for different flow geometries that are characterised by the same stretching rate factor over the same time increment (Fig. 3). For a given kinematic vorticity number W_k and a stretching rate factor S,
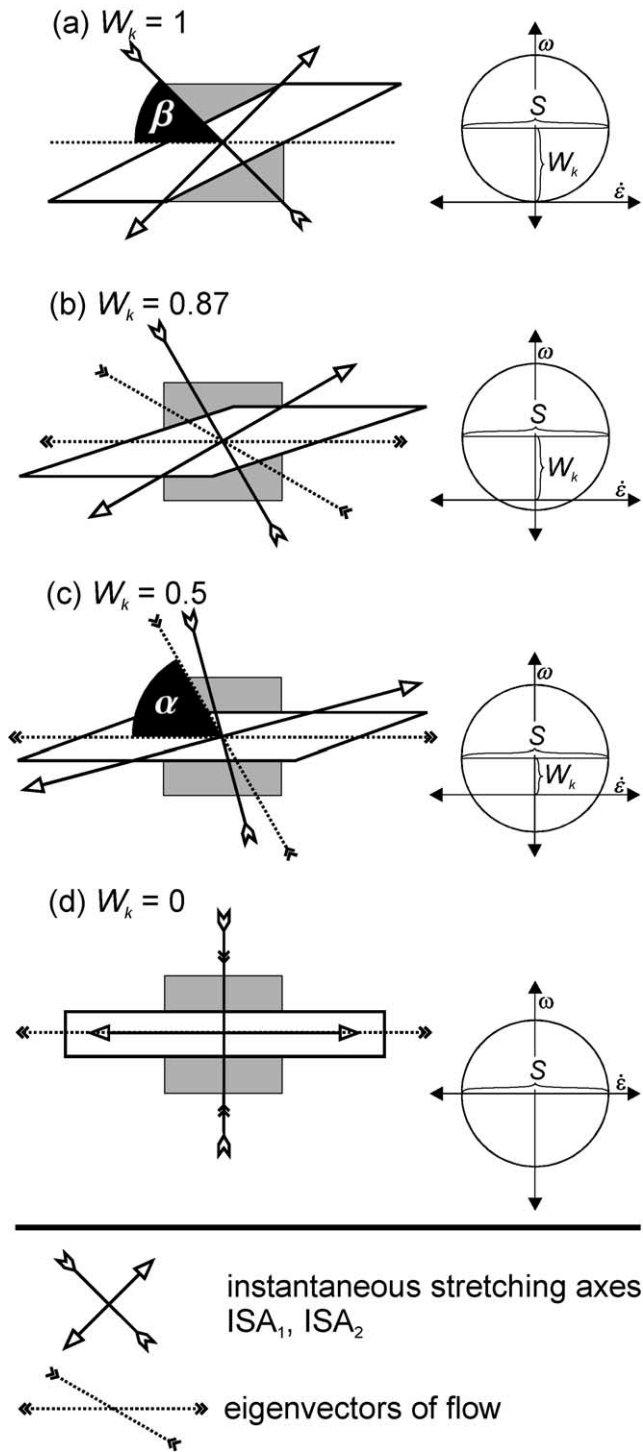
Fig. 3. Examples of finite deformation of a unit square after a time increment 1 and corresponding Mohr Circles for L having the same stretching rate factor S used in the numerical models. Examples are shown for kinematic vorticity numbers of (a) $W_k = 1$, (b) $W_k = 0.87$, (c) $W_k = 0.5$ and (d) $W_k = 0$. α is the angle between eigenvectors of flow, β is the angle between ISA$_2$ and shear zone boundary. Finite deformation parameters are given in Table 1.

the components of L can be calculated by (modified after Passchier, 1987):

$$L = \begin{pmatrix} \dfrac{S}{2}\sqrt{1 - W_k^2} & W_k S \\ 0 & -\dfrac{S}{2}\sqrt{1 - W_k^2} \end{pmatrix} \tag{5}$$

The corresponding deformation gradient tensor D given by Ramberg (1975) and combined with Eq. (6) is:

$$D = \begin{pmatrix} \exp\!\left(\dfrac{St}{2}\sqrt{1 - W_k^2}\right) & \dfrac{\sqrt{1 - W_k^2}}{2W_k} \\ 0 & \exp\!\left(-\dfrac{St}{2}\sqrt{1 - W_k^2}\right) \end{pmatrix} \tag{6}$$

where t is the time. The components of L of the different models, the derived deformation gradient tensor after $t = 1$, and the finite deformation parameters are listed in Table 1.

The boundary flow type is defined by W_k (Fig. 3), corresponding to the cosine of the angle α between the non-rotating directions (eigenvectors) of the flow (Passchier, 1987). The kinematic vorticity number consequently varies between $W_k = 0$ for ideal pure shear ($\alpha = 90°$) and $W_k = 1$ for ideal simple shear ($\alpha = 0°$). The flow type also determines the orientations of the shortening ISA$_2$ and of the stretching ISA$_1$ with respect to the shear zone boundaries, and these orientations are given by the angles β and $\beta + 90°$, respectively. The relation between α and β is given by $\beta = (\alpha + 90°)/2$. These parameters can be elegantly illustrated in a Mohr circle (e.g. Passchier, 1987) plotting instantaneous stretching rates ($\dot{\epsilon}$) against angular velocities (ω). Mohr circles of similar diameter indicate the same stretching rate factor S. Consequently, the boundary conditions used for our modelling can be illustrated by shifting a Mohr circle with a constant diameter along the ω-axis, between the end-members of pure and simple shear (Fig. 3).
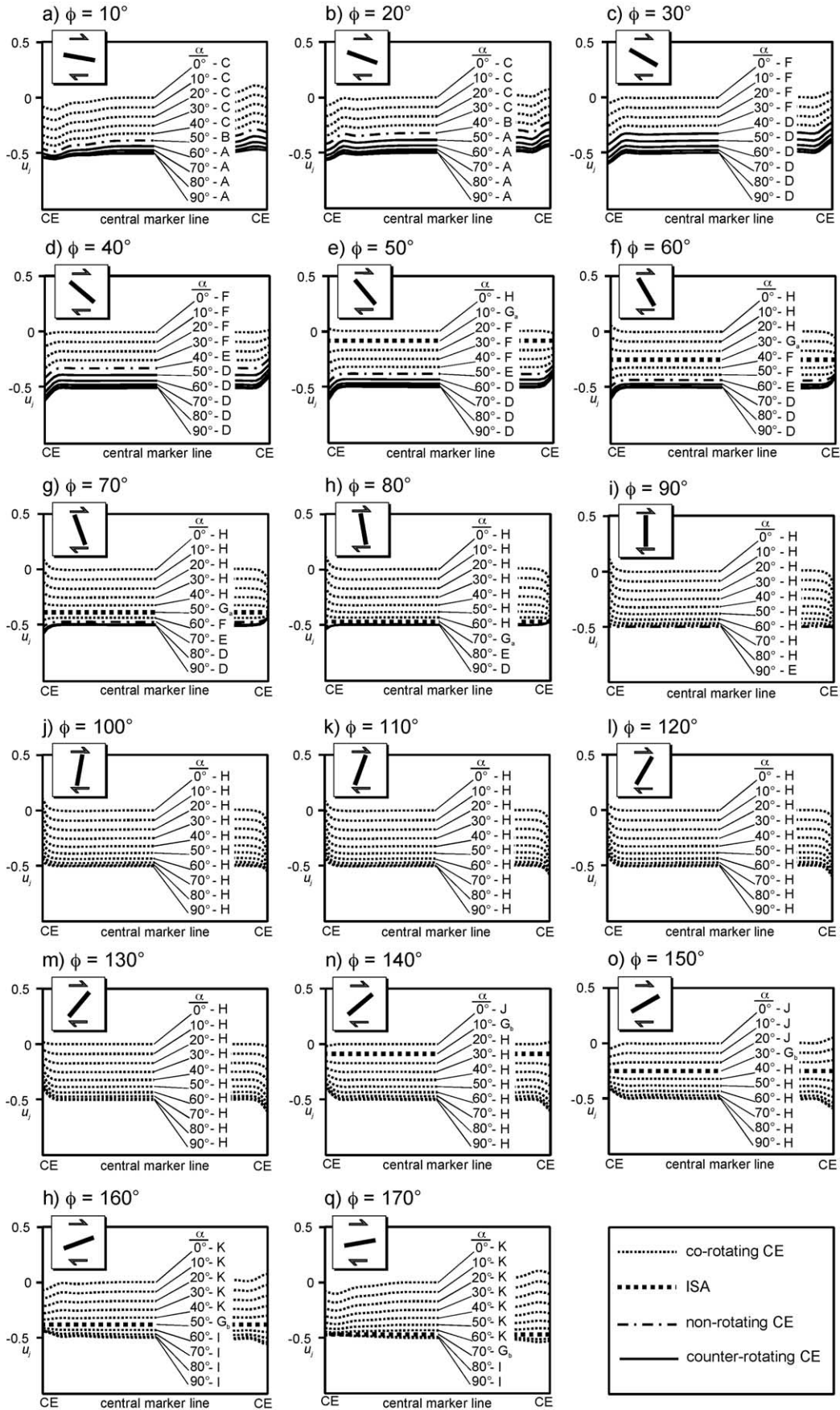
3. Instantaneous structural development

Fig. 4 shows the instantaneous deflection of the central marker line between two CEs as a function of initial orientation of the CE varying between $\phi = 10°$ and $170°$. For a given initial orientation of the CE, each diagram shows the instantaneous deflection of the central marker line for the complete range of flow types, between simple shear ($\alpha = 0°$) and pure shear ($\alpha = 90°$). The marker lines are labelled with letter codes A to K corresponding to the instantaneous flanking structures classified in Figs. 5 and 6. Different outlines are used for the central marker lines, as a function of the rotation sense of the CE, which can undergo either co-, non- or counter-rotation compared with the sense of the main shear flow. If the sense of shear along the CE is the same as the main shear flow, the slip surface is co-shearing, whereas it is counter-shearing

Table 1
List of deformation parameters of the FEM models.[a]

α	W_k	β	S	L_{ii}	L_{ij}	L_{ji}	L_{jj}	D_{ii}	D_{ij}	D_{ji}	D_{jj}	I_1	I_2	λ_1	λ_2	$1+e_1$	$1+e_2$	R
90	0	90	2	1	0	0	−1	2.718282	0	0	0.367879	7.524391	1	7.389056	0.135335	2.718282	0.367879	7.389056
85	0.087155743	87.5	2	0.996195	0.174311	0	−0.9961947	2.707958	0.204607603	0	0.369282	7.511268	1	7.375687	0.135581	2.715822	0.368213	7.375687
80	0.173648178	85	2	0.984808	0.347296	0	−0.9848077	2.677297	0.406219648	0	0.373511	7.472445	1	7.336133	0.136312	2.70853	0.369204	7.336133
75	0.258819045	82.5	2	0.965926	0.517638	0	−0.9659258	2.627219	0.601971505	0	0.380631	7.409528	1	7.272015	0.137513	2.696667	0.370828	7.272015
70	0.342020143	80	2	0.939693	0.68404	0	−0.9396926	2.559195	0.789250064	0	0.390748	7.325077	1	7.185916	0.139161	2.680656	0.373043	7.185916
65	0.422618262	77.5	2	0.906308	0.845237	0	−0.9063077	2.475167	0.965794795	0	0.404013	7.222437	1	7.081218	0.141219	2.661056	0.375791	7.081218
60	0.5	75	2	0.866025	1	0	−0.8660254	2.377443	1.129772083	0	0.42062	7.10554	1	6.961901	0.143639	2.638541	0.378997	6.961901
55	0.573576436	72.5	2	0.819152	1.147153	0	−0.8191520	2.268575	1.279818396	0	0.440805	6.978679	1	6.832315	0.146363	2.61387	0.382575	6.832315
50	0.64278761	70	2	0.766044	1.285575	0	−0.7660444	2.15124	1.415050804	0	0.464848	6.846286	1	6.696965	0.149321	2.587849	0.386421	6.696965
45	0.707106781	67.5	2	0.707107	1.414214	0	−0.7071067	2.028115	1.53504629	0	0.493069	6.712734	1	6.560302	0.152432	2.561309	0.390425	6.560302
40	0.766044443	65	2	0.642788	1.532089	0	−0.6427876	1.901775	1.639793734	0	0.525825	6.582163	1	6.426558	0.155604	2.535066	0.394467	6.426558
35	0.819152044	62.5	2	0.573576	1.638304	0	−0.5735764	1.774602	1.729624314	0	0.563506	6.458354	1	6.299614	0.15874	2.509903	0.398422	6.299614
30	0.866025404	60	2	0.5	1.732051	0	−0.5	1.648721	1.805127089	0	0.606531	6.344645	1	6.182909	0.161736	2.486546	0.402164	6.182909
25	0.906307787	57.5	2	0.422618	1.812616	0	−0.4226182	1.525952	1.86705688	0	0.655329	6.243886	1	6.079396	0.16449	2.465643	0.405574	6.079396
20	0.939692621	55	2	0.34202	1.879385	0	−0.3420201	1.407789	1.916241201	0	0.710334	6.158423	1	5.991521	0.166903	2.447758	0.408537	5.991521
15	0.965925826	52.5	2	0.258819	1.931852	0	−0.2588190	1.295399	1.953492262	0	0.771963	6.090118	1	5.921234	0.168884	2.433359	0.410955	5.921234
10	0.984807753	50	2	0.173648	1.969616	0	−0.1736481	1.189637	1.97952897	0	0.840593	6.040367	1	5.870009	0.170357	2.42281	0.412744	5.870009
5	0.996194698	47.5	2	0.087156	1.992389	0	−0.0871557	1.091067	1.99491276	0	0.916534	6.010138	1	5.838872	0.171266	2.416376	0.413843	5.838872
0	1	45	2	0	2	0	0	1	2	0	1	6	1	5.828427	0.171573	2.414214	0.414214	5.828427

[a] α—angle between eigenvectors of flow; W_k—kinematic vorticity number: $W_k = \cos\alpha$; β—angle between ISA_2 and coordinate system: $\beta = (90 + \alpha)/2$; S—stretching rate factor; L_{ij}—component of velocity gradient tensor L (fig. 2 in Passchier, 1987); D_{ij}—component of rotated general position gradient tensor with $D_{ji} = 0$ (Eq. (38) in Ramberg, 1975); I_1, I_2—first and second invariant of D (Eqs. (33.8) and (33.9) in Ramsay and Lisle, 2000); λ_1, λ_2—principal quadratic stretch (Eqs. (33.10) and (33.11) in Ramsay and Lisle, 2000); $1+_1$, $1 + e_2$—principal strain; R—ellipticity
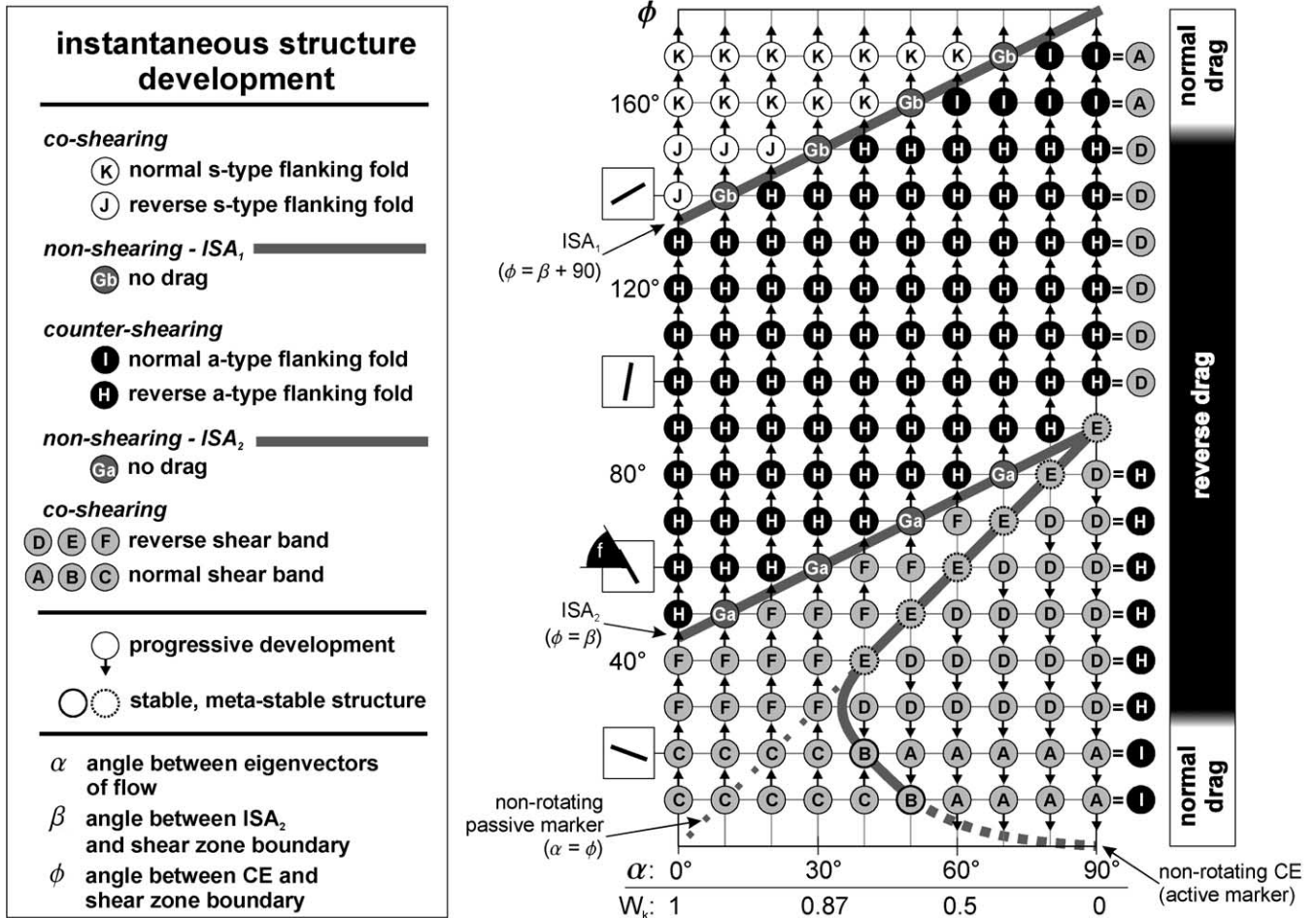
Fig. 5. Diagram illustrating the instantaneous development of flanking structures as a function of the type of flow (horizontal axis) and the initial orientation of the CE (vertical axis), based on the modelling results in Fig. 4. Letter codes A–K as in Fig. 4. See text for details.

otherwise. Faulting along the CE reveals either an extensional or contractional offset of marker lines. A key point for a correct kinematic interpretation of the flanking structure is the deflection (curvature) of marker lines in the direct vicinity of the CE. Normal-drag is defined as a deflection of the central marker line that is convex in the direction of shear along the CE, whereas a concave deflection indicates a reverse-drag (Hamblin, 1965). In other words, the drag is called 'normal' if the deflection of the central marker line indicates a rotation in accordance with the sense of shear along the CE, and is otherwise called 'reverse'.

On the basis of Fig. 4, three types of flanking structures can be distinguished (compare Fig. 1): (1) *shear bands* are co-shearing with an extensional offset; (2) *a-type flanking folds* are counter-shearing; and (3) *s-type flanking folds* are co-shearing with a contractional offset. All three types of

structures can have a normal or a reverse drag of the HE near the CE. Note that these definitions are different from those of Dennis and Secor (1987), who used normal and reverse slip for extensional and contractional offset along oblique crenulations. We emphasize that our terminology also differs from that used by Passchier (2001), who defines a flanking structure as synthetic (or antithetic) if the rotation indicated by the deflected central marker line (i.e. the drag) is in the same (or the opposite) sense with respect to the sense of shear along the CE. However, model results in Fig. 4 demonstrate that the offset along CE and the drag effects are independent parameters, both of which are necessary for the suggested terminology.

Fig. 5 together with the simplified schematic plot of Fig. 6 illustrates the instantaneous development of the various structures modelled in Fig. 4, as a function of the flow

Fig. 4. Calculated deformation of the central marker line. The diagrams show the vertical instantaneous velocity u_j plotted for the length of the central marker line between two CEs, for different flow types. The shear sense is always dextral. The initial orientations of the CE varies between $\phi = 10°$ and $170°$ (a–q). α is the angle between the eigenvectors typical for the flow type (simple shear, $\alpha = 0°$; pure shear, $\alpha = 90°$). The marker lines are labelled with letter codes A to K corresponding to the instantaneous flanking structures classified in Figs. 5 and 6. Different line patterns are used for co-, non- and counter-rotating CEs. Thick dotted lines show orientations of CEs that are parallel to either ISA$_2$ or ISA$_1$.
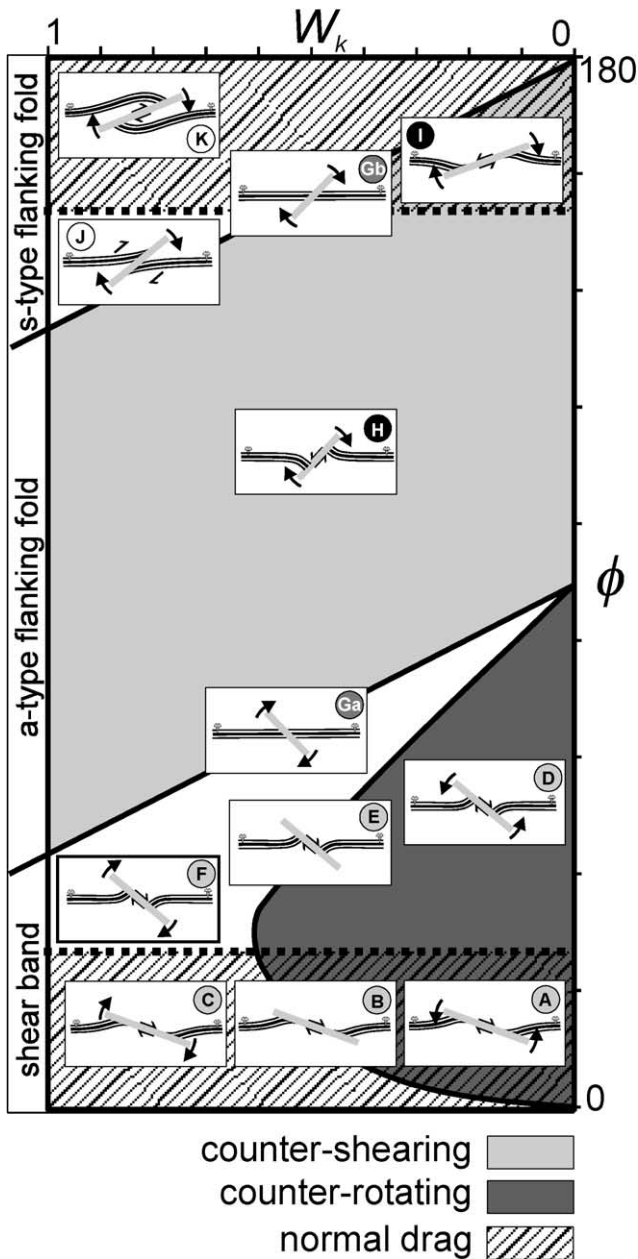
Fig. 6. Summary of the instantaneous flanking structures developing during dextral shear.

type (α) and the initial orientation of the CE (ϕ). The plot in Fig. 5 is subdivided into different fields, as a function of (i) the sense of shear along the CE, (ii) the sense of rotation of the CE; and (iii) the drag of HE.

(i) *Sense of shear along the CE*: The diagram shows three fields, separated by two oblique and parallel lines representing the orientations of the instantaneous stretching axes (ISAs) as a function of the flow type. The lower line corresponds to the shortening ISA$_2$ and its orientation is defined by $\phi = (\alpha + 90°)/2 = \beta$. The ISAs correspond to the only orthogonal pair of lines having the same angular velocity, i.e. they are directions of no infinitesimal shear. Consequently, CEs parallel to the ISA$_2$ develop no instantaneous

offset of the central marker line (structure G$_a$), although the slip surface co-rotates during progressive deformation. In the field below the ISA$_2$ ($\phi < \beta$), co-shearing along the CE leads to the development of shear bands (structures A–F), whereas counter-shearing CEs in the field above the ISA$_2$ ($\beta < \phi < \beta + 90°$) induces a-type flanking folds (structures H and I). The second direction of no instantaneous shear corresponds to the orientation of the stretching ISA$_1$, defined by $\phi = 0.5\alpha + 135° = \beta + 90°$. CEs parallel to the ISA$_1$ again develop no deflection of the central marker line (structure G$_b$). In the field above the ISA$_1$ ($\phi > \beta + 90°$), co-shearing along the CE results in the development of s-type flanking folds (structures J and K).

(ii) *Sense of rotation of the CE*: Flanking folds are always associated with co-rotating CEs but shear bands can be associated with co-, non-, or counter-rotating CEs. The orientations of non-rotating CEs (structures B and E) correspond to a curved line in the lower part of the diagram in Figs. 5 and 6. This line separates the fields of shear bands associated with co-rotating CEs, to the left (structures C and F), from those associated with counter-rotating CEs, to the right (structures A and D). For $\phi > 40°$, the line of non-rotating CEs is identical to the line of non-rotating passive markers (i.e. $\alpha = \phi$), which is by definition the orientation of the shortening eigenvector of the flow. For $\phi < 40°$, however, these lines diverge significantly, implying a field where CEs with low ϕ angles are still co-rotating, although passive markers are counter-rotating. This surprising behaviour arises because, in contrast to passive markers, the modelled CE simulates a pinned active slip surface. Transfer of material from the footwall to the hanging wall occurs at the upper slip surface tip, and from the hanging wall to the footwall at the lower slip surface tip (Barr and Houseman, 1996). If this transfer is in the direction of the bulk shear flow, the additional spin component on the CE can induce its co-rotation. However, this effect requires a significant component of co-shearing along the CE and it is consequently restricted to ϕ angles of less than 40° (Pray et al., 1997) and to deformation dominated by simple shear ($\alpha < 45°$).

(iii) *Drag of HE*: For a small initial dip of the CE ($\phi \sim < 25$–30°) the drag of the central marker line is convex in the direction of shear along the CE (i.e. normal) and the resulting structures are normal shear bands (structures A, B and C in Figs. 5 and 6). For ~ 25–30° $< \phi < \sim 150$–155°, the drag of the central marker line is reverse for all structures and flow types resulting in reverse shear bands (structures D, E and F), a-type (H) and s-type flanking folds (J). If the CE makes a very large angle with respect to the shear zone boundaries ($\phi > \sim 150$–155°), the instantaneous deformation induces again a normal drag of the central marker line and normal a-type (I) and s-type flanking folds (K) develop. However, the transition between normal and reverse drag effects is difficult to determine in the model, and might be impossible to establish in the field, inasmuch as it implies a gradual and
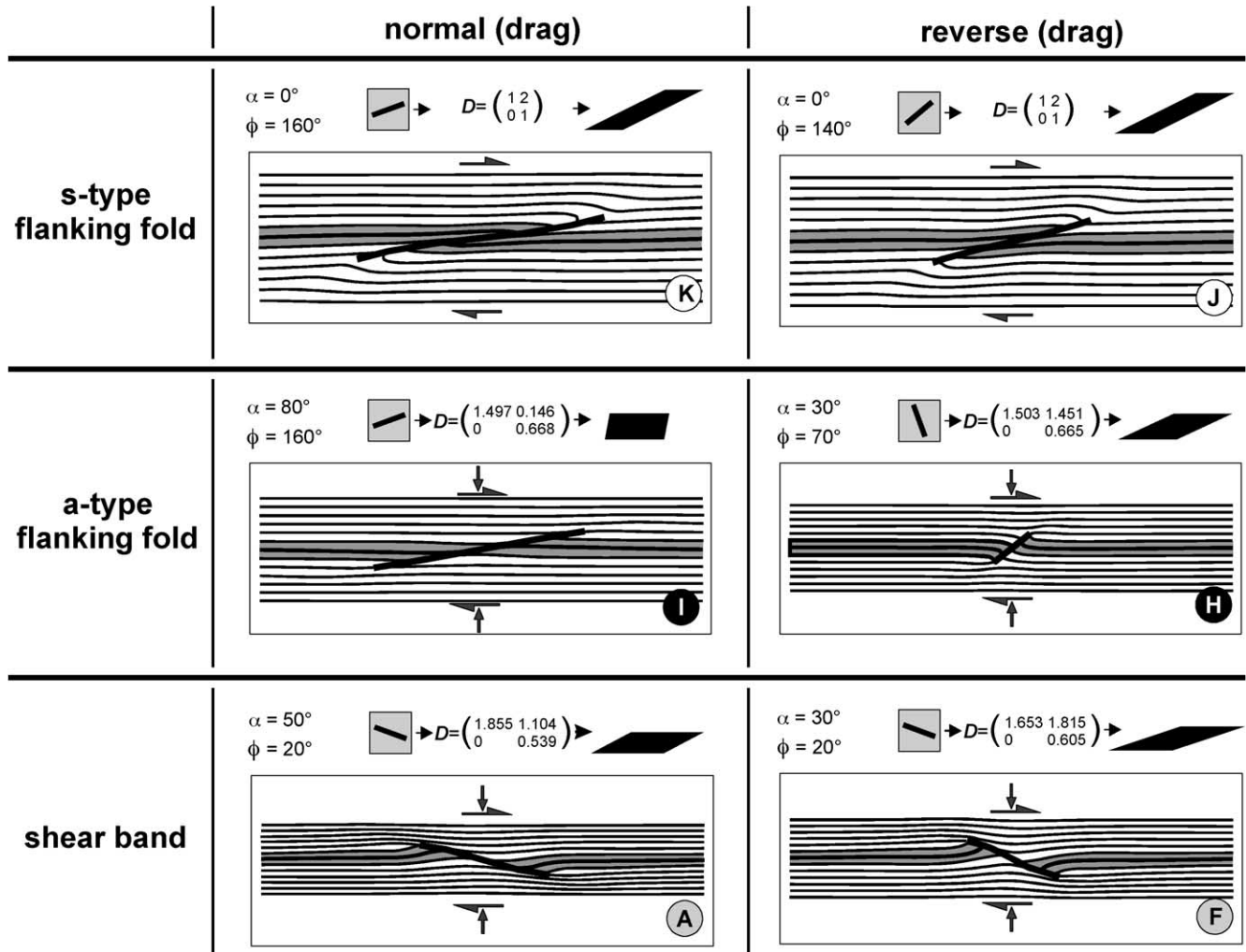
Fig. 7. Selected cases of modelled flanking structures that developed after a given finite deformation. The flow type (α), the initial orientation of the CE (ϕ) and the finite deformation tensor are shown for each case. For a detailed discussion see text.

subtle change of the deflection from convex to concave (e.g. Fig. 4a–c).

4. Finite structural development and natural examples

The results above are instantaneous solutions. Except for the special cases of non-rotating CEs (E and B), the orientation of CE will change during progressive deformation. The final structure developed will therefore depend on (i) the initial orientation of the CE, (ii) the flow type, and (iii) the finite deformation. Assuming a steady state flow (constant W_k), the small arrows in Fig. 5 indicate the direction of progressive structural evolution. Nearly all structures are unstable. During ideal simple shear ($\alpha = 0°$), for example, a normal shear band starting to develop at $\phi = 10°$ will evolve with increasing deformation to a reverse shear band (F), then to a reverse a-type flanking fold (H), to a reverse s-type flanking fold (J), and finally to a normal s-type flanking fold (K). Normal (B) and reverse shear bands (E) plotting

along the line of non-rotating CE are the only (meta-) stable structures in Fig. 5. Reverse shear bands E have, however, a precarious stability that can easily be disturbed and such structures are consequently metastable. Just a slight deviation of ϕ from its non-rotating orientation would result in either a co- or counter-rotation of the CE. On the other hand, normal shear bands B are stable structures, because a deviation from the non-rotating orientation of the CE would result in either counter- or co-rotation into the original non-rotating position. This result is consistent with the fact that normal shear bands are the most frequent structures in natural shear zones. Such natural normal shear bands are typically characterised by an angle of less than 25–30° between the CE and the main foliation, which approximates the orientation of the fabric attractor for high finite deformation (Platt and Vissers, 1980; Passchier, 1984). Our modelling is consistent with this observation as it indicates that normal drag along shear bands only develop at low $\phi < 25$–$30°$. Normal shear bands have been interpreted as being parallel to the shortening eigenvector of a general shear
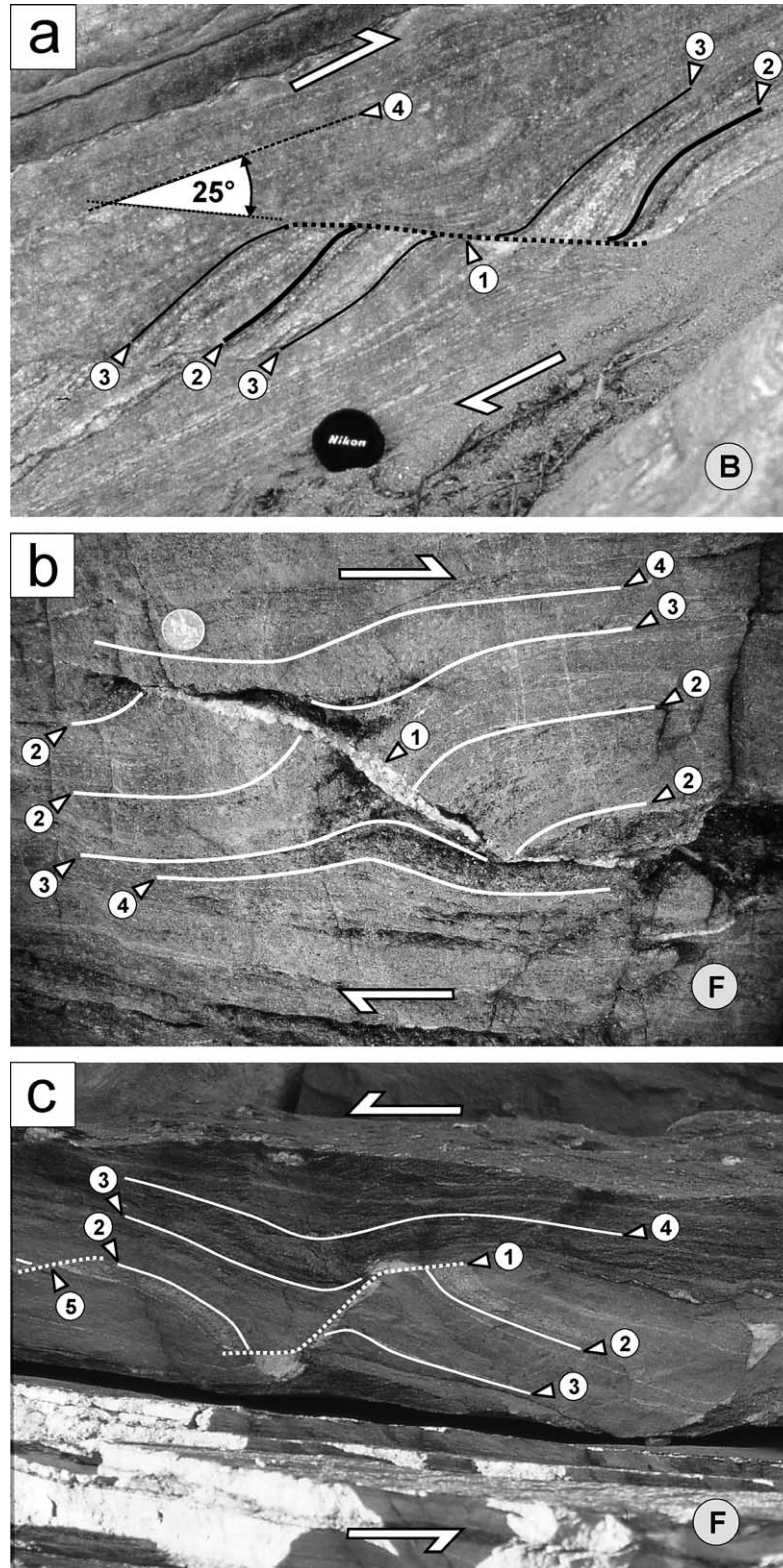
Fig. 8. (a) Normal shear band in an amphibolite facies mylonite (Sutlej Valley, NW Himalaya, N31°30′35.3″, E78°14′42.0″). [1] Co-shearing secondary shear zone (CE); [2,3] marker lines showing an extensional offset and a normal-drag; [4] main mylonitic foliation. The angle between [4] and [1] is about 25°. (b) Reverse shear band in an eclogite–amphibolite from the Eastern Alps (Schober Group, Austria, N46°55′06.9″, E12°43′10.1″). [1] Sigmoidal, co-shearing quartz vein (CE); [2] marker lines with an extensional offset and a reverse-drag; [3] marker lines revealing a normal-drag near the tips of the CE; [4] asymmetric necking of the foliation above and below the CE. (c) Reverse shear band in an amphibolite facies paragneiss (Sangla Valley, NW Himalaya, N31°26′59.5″, E78°12′29.9″). [1] Sigmoidal, co-shearing quartz vein (CE); [2] calc–silicate marker horizon with an extensional offset and a reverse-drag; [3] marker lines revealing a normal-drag near the tips of the CE; [4] leading edge fold; [5] calc–silicate marker horizon boudinaged by a normal-drag shear band.

flow (Simpson and De Paor, 1993; Pray et al., 1997). In contrast, our modelling shows that stable normal shear bands develop where CE is less steep than the shortening eigenvector of the flow, and that CEs parallel to the shortening eigenvector are either unstable or metastable. In the following sections the various types of flanking structures simulated by our numerical model are compared with natural structures.

4.1. Shear bands (co-shearing slip surfaces with extensional offset)

(i) *Normal shear bands* are characterised by a convex drag of the central marker line towards the shear sense along the CE (Fig. 7) and consequently the deflection is consistent with a drag along the co-shearing CE. It should be noted that strictly speaking the normal-drag in the direct vicinity of the CE is superposed on a reverse drag further away from the CE. Typical natural examples of normal shear bands are illustrated in many publications (e.g. shear bands from many different rock types developed under a broad range of metamorphic conditions are found in Snoke et al. (1998)). Although such structures are commonly used as a kinematic indicator, we emphasize, again, that they are not always easily distinguished from a-type flanking folds related to an opposite shear sense, and such structures have been occasionally confused (Grasemann and Stüwe, 2001). Fig. 8a shows a normal shear band in a mylonite of the Main Central Thrust (NW Himalayas) characterised by a well-defined shear sense (Vannay and Grasemann, 1998). The CE [1] corresponds to a co-shearing slip surface recording an extensional offset. The convex deflection of the marker lines [2,3] in the direct vicinity of the CE indicates a normal drag superposed on a reverse drag away from the CE. In such a highly-deformed mylonite, the 25° angle between the CE and the mylonitic foliation, parallel to the shear zone boundaries, strongly suggests a stable normal shear band (structure B in Fig. 6) that developed in a general shear flow characterised by an intermediate W_k ($0.6 \leq W_k \leq 0.8$), in good agreement with quantitative kinematic indicators reported from the Main Central Thrust (Grasemann et al., 1999).

(ii) *Reverse shear bands* are characterised by concave drag of the central marker line. These structures are identical to the asymmetric foliation boudinage revealing a reverse drag effect (fig. 4 in Platt and Vissers, 1980). The transition between normal and reverse shear bands is not easy to determine. Although the distinction between these structures gets clearer after some finite deformation (Fig. 7), a correct identification of shear bands requires a careful inspection of the deflection of the central marker line. Furthermore, reverse shear bands and reverse a-type flanking folds are confusingly similar, potentially resulting in an incorrect shear sense interpretation. Natural examples of reverse shear bands from an eo-Alpine eclogite–amphibolite and from an amphibolite facies paragneiss from the

Main Central Thrust (NW Himalayas) are illustrated in Fig. 8b and c, respectively. In both examples the shear sense is well-established by independent shear sense criteria. Both structures consist of a co-rotating CE corresponding to an apparently weak quartz-filled vein [1], cutting at a relatively large angle the more competent metamorphic foliation. Whereas most of the marker lines reveal a reverse-drag [2], marker lines at the lower part of the footwall of the CE, as well as at the upper part of the hanging wall of the CE, show a normal-drag [3]. Together with the relatively large angle between the CE and the marker horizons, this change of the marker lines drag along the CE is a specific characteristic of reverse shear bands. Furthermore, the CE is folded consistently with the bulk shear sense. Extension along the CE is compensated by asymmetric necking of the foliation above and below the vein [4]. These characteristics can be also observed in the FEM model results plotted in Fig. 7.

Because we modelled a pinned slip surface with co-shearing slip, the CE is deformed in both types of shear bands (Barr and Houseman, 1992). This deformation results in a sigmoidal shape of the CE that is consistent with the boundary shear sense. Such a sigmoidal CE is also typical for natural shear bands, suggesting that such structures may also not freely propagate in real rocks. The orientation of the sigmoidal shape may also serve as an important characteristic to distinguish between shear band and a-type flanking folds.

4.2. a-Type flanking folds (counter-shearing slip surfaces)

(i) *Reverse a-type flanking folds* reveal a drag of the central marker line that is concave towards the shear sense along the CE and these structures are equivalent to the 'paired hook folds' described by Hudleston (1989). Due to the diminishing amount of offset along the CE, the amplitude of the flanking folds decreases from the central marker line towards the tips of the CE. The marker lines above and below the pinned tips of the CE typically form leading edge folds characterised by a vergence that is inconsistent with the boundary shear sense. For CEs oriented at $90° < \phi < 135°$ with respect to the shear zone boundaries, reverse a-type flanking folds will develop in all types of flow between simple shear to pure shear and such structures are probably much more common than currently reported. Fig. 9a illustrates a typical reverse a-type flanking fold developed in a calcite mylonite from the detachment fault of the Naxos metamorphic core complex, characterised by unambiguous shear sense (Buick, 1991). The CE corresponds to a late slip surface, cutting the layering and mylonitic foliation [1], and subsequently co-rotated during progressive deformation. All the marker horizons [3] cut by the co-shearing slip surface [1], including the central marker line [2], show an extensional offset and a reverse-drag. The marker lines above and below the slip surface tips [4] are slightly folded but they show no offset in the continuation of the slip
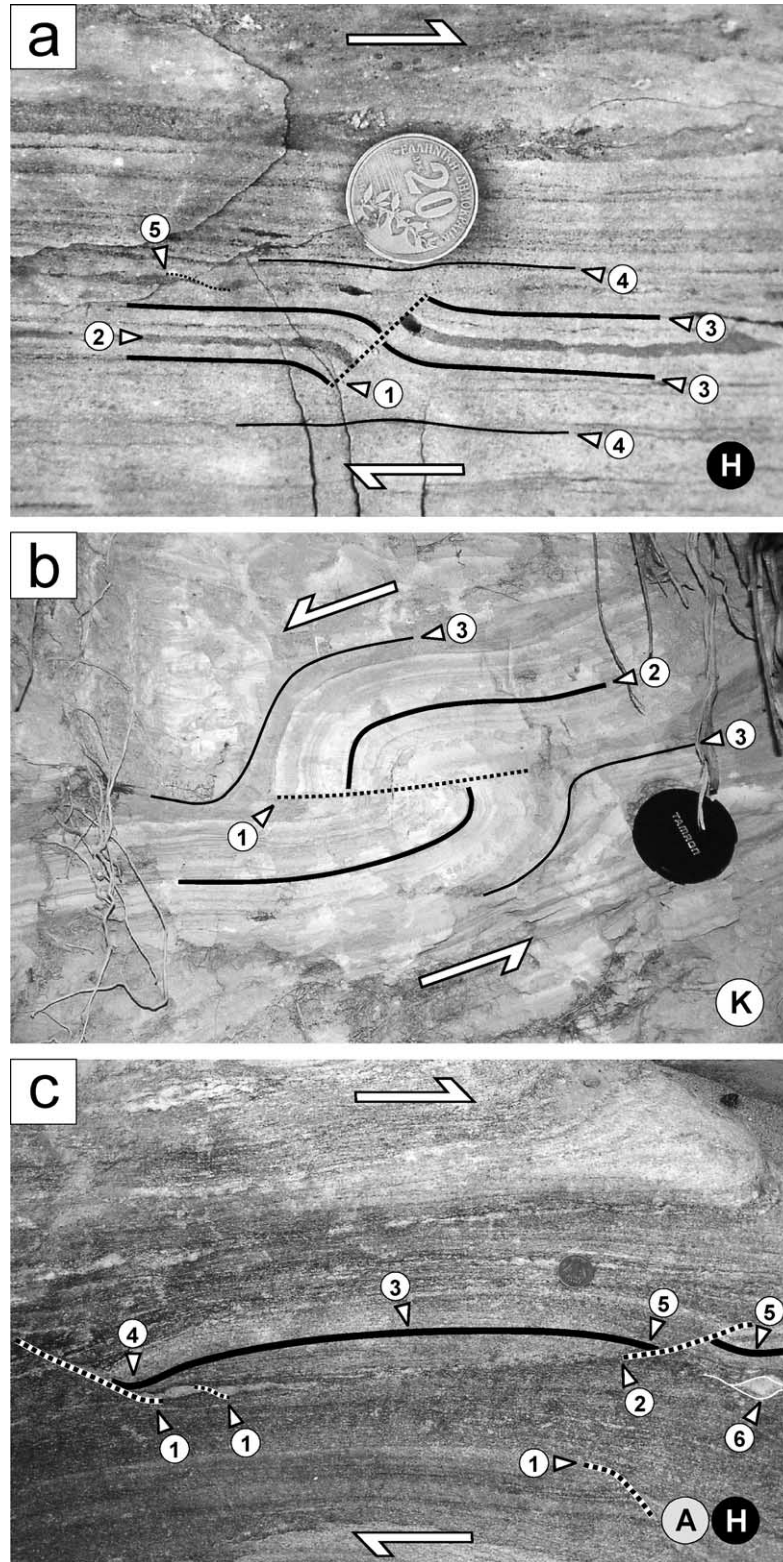
Fig. 9. (a) Reverse a-type flanking folds in a mylonitic marble from Naxos (Greece, N37°11′23.6″, E25°30′55.1″). [1] Counter-shearing fault (CE); [2] central marker line and [3] marker lines showing an extensional offset and a reverse-drag; [4] leading edge folds; [5] normal-drag shear band. (b) Normal s-type flanking fold in Quaternary lake sediments from the NW-Himalaya (Sangla Valley, India, N31°26′03.7″, E78°14′20.9″). [1] Co-shearing CE; [2] central marker line showing a contractional offset and a normal-drag; [3] leading edge folds. (c) Conjugate set of dextral flanking structures in an amphibolite facies mylonite (Sutlej Valley, NW Himalaya, N31°30′24.3″, E78°14′01.0″). [1] Co-shearing extensional CE associated with normal shear band; [2] counter-shearing extensional CE associated with reverse a-type flanking fold; [3] central marker line; [4] normal-drag along the shear band; [5] reverse-drag along the a-type flanking fold; [6] σ-type feldspar clast indicating dextral shear.

reverse a-type flanking fold

α = 90°
φ = 110°

$$D = \begin{pmatrix} 1.801 & 0 \\ 0 & 0.555 \end{pmatrix}$$

H

reverse shear band

α = 90°
φ = 70°

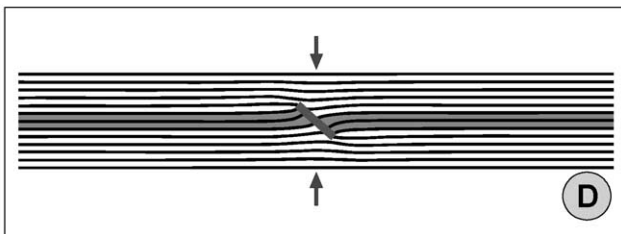$$D = \begin{pmatrix} 1.801 & 0 \\ 0 & 0.555 \end{pmatrix}$$

D
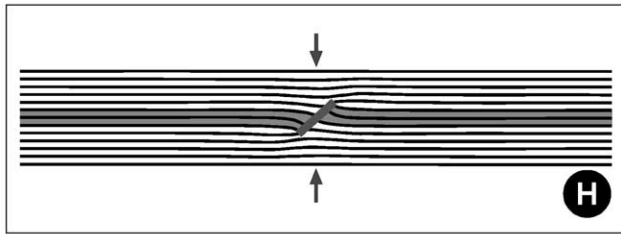
Fig. 10. Finite reverse a-type flanking fold ($\phi = 110°$) and reverse shear band ($\phi = 70°$) showing exact mirror symmetry after pure shear deformation.

surface. Note that these gentle leading edge folds have a vergence that is inconsistent with the bulk shear sense. The straight CE, the consistent drag of all the marker lines cut by the CE, and the dextral shear sense confirmed by normal-drag shear band boudinage [5] are the features distinguishing this structure from a reverse shear band.

(ii) *Normal a-type flanking folds* share several similarities with normal shear bands, namely the extensional offset and normal drag of marker lines. Such structures may consequently be difficult to distinguish in natural examples. Normal a-type flanking folds should not be frequently observed in nature because such structures develop only in shear flows dominated by pure shear, and they evolve to normal s-type flanking folds during progressive deformation (Fig. 5). It is interesting to note, however, that normal a-type flanking folds and normal shear bands can both develop together, leading to co-existing structures looking like a conjugate set of normal shear bands indicative of pure shear dominated flow (Platt, 1984; Harris and Cobbold, 1985; Grasemann et al., 1999).

Shear bands and a-type flanking folds, especially with reverse drag, are difficult to distinguish. This similarity between reverse shear bands and a-type flanking folds becomes clear, when the model is deformed under ideal pure shear conditions (Fig. 10). Because the deformation is coaxial a model with an initial CE oriented with an angle $\phi = 110°$ would be an exact mirror image of the

same model using $\phi = 70°$. Therefore, under pure shear deformation, structures D = H (and also A = I; see Fig. 5). For these initial orientations of CEs, however, even a small dextral non-coaxial component applied at the shear zone boundaries would result in the development of reverse a-type flanking folds and reverse shear bands, respectively.

4.3. s-Type flanking folds (co-shearing slip surfaces with contractional offset)

(i) *Normal s-type flanking folds* are characterised by co-shearing contractional offset at the level of the central marker line, which decreases towards zero at the tips of the CE. Above and below the pinned tips of the CE, leading edge folds with a vergence consistent to the sense of the bulk shear flow develop (Boyer, 1986). Normal s-type flanking folds reveal several similarities with fault-propagation-folds (Suppe and Medwedeff, 1984), although the modelled pinned slip surface can by definition not propagate. The main analogy stems from the fact that the CE cuts up-section through the syncline of the leading edge folds and that it records a decreasing displacement towards its tips. Although fault-propagation-folds normally grow as a thrust ramp propagates up-section from a bedding-parallel fault segment, observations by McConnell et al. (1997) support the interpretation that such faults can also develop both up- and down-dip from a nucleation point. The development of folds above fault tips will be favoured when the rate of fault growth is low relative to the slip rate (Suppe and Medwedeff, 1984) or when the fault tip is pinned as the fault slip increases (Wickham, 1995). Although there are many natural examples of structures that could represent s-type flanking folds, it is difficult to demonstrate that the formation of the folds is a direct consequence of co-shearing along a co-rotating CE, and not of shearing of the overturned limb of an antiform–synform fold train. An exceptionally beautiful example of a 'rootless fold' is given in fig. 7 of Martelat et al. (1997), where a clearly-developed leading edge fold supports the interpretation of this structures as a normal-drag s-type flanking fold. Fig. 9b shows a natural case of a possible normal s-type flanking fold in Quaternary lake sediments from the Himalaya. The CE corresponds to a discrete slip surface [1], possibly representing the reactivation of one of the high-angle extensional faults commonly observed in these sediments. The fine layering clearly reveal the contractional offset of the central marker line [2] at the level of the CE, whereas the marker lines above and below the slip surface tips [3] developed a continuous antiform–synform fold train. The down-dip vergence of these leading edge folds indicates that the structure formed during tilting and slumping of these soft sediments. As the slip surface is not continuing in a decollement level this structure did not develop as a fault-propagation-fold and the interpretation of a s-type flanking fold is favoured.

(ii) *Reverse s-type flanking folds* will evolve to normal s-type flanking folds during progressive deformation.

However, the difference in the drag of the marker line is subtle and the transition from reverse to normal s-type flanking folds would probably be difficult to distinguish in the field. In both modelled examples of s-type flanking folds (Fig. 7), the CE is deformed as a direct consequence of the slip along a pinned slip surface (Barr and Houseman, 1992).

5. Discussion

5.1. Are flanking structures useful (quantitative) kinematic indicators?

Shear bands have been abundantly used as kinematic indicators, although several observations have suggested a more cautious use of this shear sense criteria (Platt and Vissers, 1980; Behrmann 1987; Grasemann and Stüwe, 2001). The results of the present study emphasize this warning by showing that both types of shear bands can be nearly mirror images of a-type flanking folds recording an opposite shearing direction. This pessimistic view has to be considered, however, parallel with the fact that normal shear bands often appear to successfully record the correct shear sense constrained by other independent criteria. Moreover, our mechanical modelling shows that, if correctly analysed and interpreted, well-developed flanking structures can not only be useful shear sense criteria, but that they can also provide information about the flow type, as discussed in the following paragraph.

Normal shear bands are characterised by a low angle with respect to the shear zone boundaries, as well as by a clear deflection of the marker lines that is consistent with the shear sense along the CE. In good agreement with the results of our modelling, natural examples of normal shear bands are typically characterised by an angle of less than 25–30° between the CE and the main foliation, which is probably close to the fabric attractor (e.g. Berthé et al., 1979; Platt and Vissers, 1980; Passchier, 1984). Although normal shear bands can form in all types of flow, such structures are only stable in a general flow characterised by W_k around 0.6–0.8 ($\alpha = 40$–$50°$). Natural normal shear bands can be very difficult, or even impossible to distinguish from *normal a-type flanking folds* if the deflection of marker lines is not clearly exposed. In highly-strained rocks, however, a pronounced offset of the central marker line at the level of the CE is most likely indicative of normal shear bands (Fig. 7). Furthermore, CEs associated with normal shear bands should have a sigmoidal shape, whereas CEs associated with normal a-type flanking folds should be straight (Fig. 7).

Reverse shear bands and *reverse a-type flanking folds* are difficult to distinguish and it will be impossible to deduce the shear sense from one structure alone. A close interlimb angle of the folds along the CE could indicate a reverse a-type flanking fold, because folds associated with reverse shear band always show open angles between the limbs,

even after high deformation (Baumann, 1986). If it can be shown that the CE is counter-rotating, then the structures are reverse shear bands and the flow must have had a significant component of pure shear. Moreover, the CE should be sigmoidal in reverse shear bands and more straight in reverse a-type flanking fold (Fig. 7).

Reverse and *normal s-type flanking folds* are the only structures recording a contractional offset of the central marker line and they are therefore good shear sense indicators. The development of s-type flanking structures is favoured by simple shear deformation.

5.2. Conjugate flanking structures

Natural examples of conjugate shear bands have been interpreted to be indicative of a strong coaxial component of deformation (e.g. Platt, 1984). According to our model, various combinations of shear bands coexisting with either a-type flanking folds or s-type flanking folds can develop as a function of the initial orientation of the CE, the flow type and the finite deformation. Such conjugate structures are unlikely to be common in ductile flows dominated by simple shear ($\alpha < 30°$), inasmuch as shear bands are unstable for such a flow and they evolve to flanking folds with increasing deformation. Alternatively, combinations of reverse a-type flanking folds with either reverse or normal s-type flanking folds can develop in flows dominated by simple shear. In ductile flows dominated by pure shear ($\alpha > 50°$), conjugate sets of shears bands and a-type flanking folds are more likely to be observed, inasmuch as these structures are associated with CEs characterised by opposite rotation directions, and shear bands can be stable. It is therefore probable that at least some of the 'conjugate shear bands' described in the literature rather correspond to combinations of normal and/or reverse shear bands with a-type flanking folds.

Fig. 9c shows a natural example of a conjugate set of dextral flanking structures in a mylonite from the Main Central Thrust (NW Himalaya), where the shear sense is clearly defined. The normal shear band is associated with a co-shearing extensional CE [1] along which the central marker line [3] shows a normal drag [4]. The same central marker line [3] indicates a reverse-drag [5] along the counter-shearing extensional CE [2] associated with the reverse a-type flanking fold. The dextral shear sense is independently supported by a σ feldspar clast [6]. The development of such a conjugate set of flanking structures is indicative of a general flow dominated by pure shear, which is again in good agreement with quantitative kinematic analysis of structures from the Main Central Thrust (Grasemann et al., 1999).

5.3. Does the development of flanking structures require a pre-existing anisotropy?

Analogue models suggest that shear bands form in HEs with a pre-existing anisotropy like layering or foliation (e.g.

Williams and Price, 1990). Although anisotropy might be important for the formation of CEs (Platt and Vissers 1980; Dennis and Secor, 1987), our study demonstrates that all flanking structures can develop in perfectly homogeneous host rocks, provided that CEs exist or can develop and that slip is allowed along the CEs. Although shear band structures are frequently developed in highly-foliated rocks, flanking structures may also develop in non-layered rocks like quartzites or marbles (e.g. Grasemann and Stüwe, 2001, fig. 6b). However, the identification of shear bands and flanking folds in such 'homogeneous' rocks could be hindered by the lack of marker horizons.

5.4. Does the orientation of flanking structures relate to planes of maximum finite shear strain?

Recently, it has been suggested that secondary ductile shear zones may relate to planes of maximum finite shear strain (Ramsay and Lisle, 2000). During simple shear flow two sets of structures may develop, a counter-shearing *C1-band* and a co-shearing *C2-band*, both of which are dipping in the opposite direction relative to the bulk shear. According to our model these orientations would develop a-type (C1-bands) and s-type (C2-bands) flanking folds. However, shear bands, which are co-shearing but dipping in the direction of bulk shear flow, are the most frequent flanking structures and have been successfully applied as shear sense criteria (for examples see Passchier and Trouw, 1996). Because of their orientation these shear bands cannot be related to planes of maximum finite shear strain. Yet again, a precise distinction between C1 bands (a-type flanking folds) and shear bands are crucial for the correct interpretation of the shear sense, which might be aided by a careful comparison of natural examples with modelled finite structures outlined in Section 4.

6. Conclusions

The instantaneous geometry of flanking structures is a function of the initial orientation of the CE and the flow field. On the basis of the shear sense along the CE, and offset of the HE, flanking structures can be separated into shear bands, a- and s-type flanking folds, all of which can have a normal and reverse drag. Shear bands and a-type flanking folds can be easily confused in natural rocks, potentially resulting in an incorrect kinematic interpretation. During progressive deformation, most flanking structures gradually evolve to other types of flanking structures as a consequence of rotation of the CE. Normal shear bands with low angle orientations of the CE, which is non-rotating, are the only stable structures. The stability of normal shear bands, predicted by our modelling, accounts for the fact that this type of flanking structure is the most common in nature and has been successfully used as shear sense indicator. The present modelling indicates that conjugate shear bands can develop only during pure shear, when shear bands and

a-type flanking folds are mirror images. Non-coaxial deformation can result in conjugate sets of shear bands and flanking folds. Flanking structures can form in homogeneous host rocks, without the need for pre-existing anisotropies or layering, provided that CEs already exist or can develop.

References

Barr, T.D., Houseman, G.A., 1992. Distribution of deformation around a fault in a non-linear ductile medium. Geophysical Research Letters 19, 1145–1148.

Barr, T.D., Houseman, G.A., 1996. Deformation fields around a fault embedded in a non-linear ductile medium. Geophysical Journal International 125, 473–490.

Baumann, M.T., 1986. Verformungsverteilung an Scherzonenenden: Analogmodelle und natürliche Beispiele. Unpublished PhD thesis, ETH, Zürich.

Behrmann, J.H., 1987. A precautionary note on shear bands as kinematic indicators. Journal of Structural Geology 9, 659–666.

Berthé, D., Choukroune, P., Jegouzo, P., 1979. Orthogneiss, mylonite and non coaxial deformation of granites: the example of the South Armorican shear zone. Journal of Structural Geology 1, 31–43.

Boyer, S.E., 1986. Styles of folding within thrust sheets: examples from the Appalachians and Rocky Mountains of the USA and Canada. Journal of Structural Geology 8, 325–339.

Buick, I.S., 1991. Mylonitic fabric development on Naxos. Journal of Structural Geology 13, 643–655.

Dennis, A.J., Secor, D.T., 1987. A model for the development of crenulation in shear zones with applications from the Southern Appalachian Piedmont. Journal of Structural Geology 9, 809–817.

Fossen, H., Tikoff, B., 1997. Forward modeling of non-steady-state deformations and the "minimum strain path". Journal of Structural Geology 19, 987–996.

Grasemann, B., Stüwe, K., 2001. The development of flanking folds during simple shear and their use as kinematic indicators. Journal of Structural Geology 23, 715–724.

Grasemann, B., Fritz, H., Vannay, J.C., 1999. Quantitative kinematic flow analysis from the Main Central Thrust Zone (NW-Himalaya, India):

implications for a decelerating strain path and the extrusion of orogenic wedges. Journal of Structural Geology 21, 837–853.

Hamblin, W.K., 1965. Origin of "reverse drag" on the down-thrown side of normal faults. Geological Society of America Bulletin 76, 1145–1164.

Harris, L.B., Cobbold, P.R., 1985. Development of conjugate shear bands during bulk simple shearing. Journal of Structural Geology 7, 37–44.

Hudleston, P.J., 1989. The association of folds and veins in shear zones. Journal of Structural Geology 11, 949–957.

Jiang, D., 1998. Forward modeling of non-steady-state deformations and the 'minimum strain path': discussion. Journal of Structural Geology 20, 975–977.

Jiang, D., White, J.C., 1995. Kinematics of rock flow and the interpretation of geological structures with particular reference to shear zones. Journal of Structural Geology 17, 1249–1266.

Mancktelow, N.S., 1991. The analysis of progressive deformation from an inscribed grid. Journal of Structural Geology 13, 859–864.

Martelat, J.-E., Nicollet, C., Lardeaux, J.-M., Vidal, G., Rakotondrazafy, R., 1997. Lithospheric tectonic structures developed under high-grade metamorphism in the Southern part of Madagascar. Geodinamica Acta 10, 94–114.

McConnell, D.A., Kattenhorn, S.A., Benner, L.M., 1997. Distribution of fault slip in outcrop-scale fault-related folds, Appalachian Mountains. Journal of Structural Geology 19, 257–267.

Odonne, F., 1990. The control of deformation intensity around a fault: natural and experimental examples. Journal of Structural Geology 12, 911–921.

Passchier, C.W., 1984. The generation of ductile and brittle shear bands in a low angle mylonite zone. Journal of Structural Geology 6, 273–281.

Passchier, C.W., 1987. Efficient use of the velocity gradient tensor in flow modelling. Tectonophysics 136, 159–163.

Passchier, C.W., 2001. Flanking structures. Journal of Structural Geology 23, 951–962.

Passchier, C.V., Trouw, R.A.J., 1996. Microtectonics. Springer, Berlin.

Platt, J.P., 1984. Secondary cleavages in ductile shear zones. Journal of Structural Geology 6, 439–442.

Platt, J.P., Vissers, R.L.M., 1980. Extensional structures in anisotropic rocks. Journal of Structural Geology 2, 397–410.

Pray, J.R., Secor Jr, D.T., Sacks, P.E., Maher, J.H.D., 1997. Rotation of fabric elements in convergent shear zones, with examples from the southern Appalachians. Journal of Structural Geology 19, 1023–1036.

Ramberg, H., 1975. Particle paths, displacement and progressive strain applicable to rocks. Tectonophysics 28, 1–37.

Ramsay, J.G., Lisle, R.J., 2000. The Techniques of Modern Structural Geology. Volume 3: Applications of Continuum Mechanics in Structural Geology. Academic Press, London.

Reches, Z., Eidelman, A., 1995. Drag along faults. Tectonophysics 247, 145–156.

Simpson, C., De Paor, D., 1993. Strain and kinematic analysis in general shear zones. Journal of Structural Geology 15, 1–20.

Snoke, A.W., Tullis, J., Todd, V.R., 1998. Fault-related Rocks. Princeton University Press, Princeton, NJ.

Stock, P., 1992. A strain model for antithetic fabric rotation in shear band structures. Journal of Structural Geology 14, 1267–1275.

Suppe, J., Medwedeff, D.A., 1984. Fault-propagation folding. Geological Society of America Abstracts with Programs 16, 670.

Vannay, J.C., Grasemann, B., 1998. Himalayan inverted metamorphism in the High Himalaya of Kinnaur (NW India): petrography versus thermo-barometry. Schweizer mineralogische und petrographische Mitteilungen 78, 107–132.

White, S., 1979. Large strain deformation: report on a Tectonic Studies Group discussion meeting held at Imperial College, London on 14 November 1979. Journal of Structural Geology 1, 333–339.

Wickham, J., 1995. Fault displacement-gradient folds and the structure at Lost Hills, California (USA). Journal of Structural Geology 17, 1293–1302.

Williams, P.F., Price, G.P., 1990. Origin of kinkbands and shear-band cleavage in shear zones; an experimental study. Journal of Structural Geology 12, 145–164.